Article

Controlled Growth of Vertically Aligned Nanocomposites through a Au Seeding-Assisted Method

Jianan Shen, Zedong Hu, Lizabeth Quigley, and Haiyan Wang*

Read Online

ACCESS | Metrics & More | Article Recommendations | Supporting Information

ABSTRACT: Heteroepitaxial metal-oxide vertically aligned nano-composites (VAN) have piqued significant interest due to their remarkable vertical interfacial coupling effects, strong structural and property anisotropy, and potential applications in magnetoelectrics, photocatalysts, and optical metamaterials. VANs present a unique pillar-in-matrix structure with uniform but rather random pillar distributions. Achieving a well-controlled pillar growth remains a major challenge in this field. Here, we use $BaTiO_3$ (BTO)-Au as a model VAN system to demonstrate the effects of Au seedings on achieving such pillar-growth control with enhanced ordering and morphology tuning. The Au seedings are introduced using an anodic aluminum oxide (AAO) template through pulsed laser deposition (PLD). TEM characterization reveals that the Au seedings result in straighter and more evenly distributed Au pillars in the BTO matrix compared to those without seeding, with the diameter of the Au seedings increasing with the number of pulses. Additionally, spectroscopic ellipsometry demonstrates distinct permittivity dispersion for all samples. This demonstration lays a foundation for future controlled and selective growth of VAN systems for on-chip integration.

Step 1: Au seedings deposition → Step 2: VAN deposition
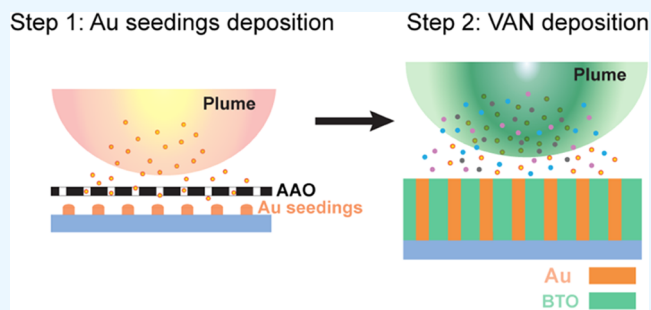
1. INTRODUCTION

Self-assembled metal-oxide nanocomposites have generated tremendous research interest due to their fascinating functionalities and potential applications in the fields of energy harvesting devices, catalysis, magnetic data storage, and optical metamaterials.[1−8] Among them, vertically aligned nano-composites (VAN) with metal nanopillars embedded in an oxide matrix have attracted much attention because of their vertical strain coupling, strong structural and property anisotropy, enabling the epitaxial growth of large mismatched systems, and versatile material combinations coupling spin, charge, lattice, and orbital degrees of freedom.[9,10] However, due to the limited understanding of the growth kinetics in the self-assembly VAN growth process, controlling the morphology of the formed nanopillars by simply tuning the deposition parameters is usually difficult. Very uniform pillar distribution and density tuning have been demonstrated in multiple VAN systems, but with limited success in achieving ordering and morphology control of nanopillars.[11−13] Lu et al. demonstrated initial success in in-plane long-range ordering in the $La_{0.7}Sr_{0.3}MnO_3$-Au system on annealed $SrTiO_3$ (STO) substrates with well-controlled terraces for nucleation.[11] Aimon et al. developed a method for templating $BiFeO_3$/$CoFe_2O_4$ VAN based on selective nucleation in the surface topography features of the substrate produced by focused ion beam (FIB) technique.[12] Furthermore, an anodic aluminum oxide (AAO) template was thinned to sub-micron level and used to successfully construct Fe_3O_4/$BaTiO_3$ (BTO) nano-

pillar composites by Dong et al., where the AAO was later etched away by NaOH.[13] Besides, there are other reports utilizing a combination of e-beam lithography (EBL) and reactive ion etching to template the substrate resulting in patterned self-assembly nanocomposites.[14,15] However, these methods are either expensive and complex in nature (e.g., EBL and FIB) or involve chemical agents to remove the physical template (e.g., AAO), leaving chemical residue on the sample.[16,17] Hence, a simple and clean method is needed to achieve an enhanced in-plane ordering and morphology control of the nanopillars in the matrix.

Recently, several studies have showcased the potential of employing a self-assembled buffer layer as a template to enhance the pillar-in-matrix structure. Zhang et al. utilized a TiN-Au buffer layer as a foundation for growing ordered and straight Au pillars within an HfO_2 matrix.[18] Similarly, Misra et al. achieved a highly ordered Au-BTO-ZnO three-phase "nanoman" structure by implementing a two-step templated growth approach, where a BTO-Au layer was first grown on the substrate, followed by subsequent BTO-ZnO growth.[19]
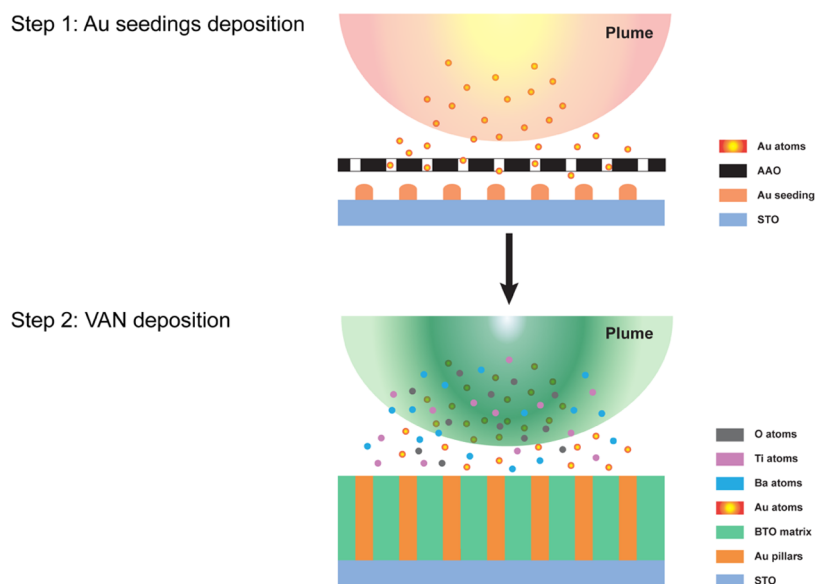
Figure 1. Schematic diagram illustrating the deposition process of the Au seedings and the subsequent BTO-Au film.

Drawing inspiration from these successful endeavors, we have adopted a two-step pulsed laser deposition (PLD) growth process to achieve precise control over the growth of the BTO-Au nanocomposite thin film, as illustrated in Figure 1. Specifically, in Step 1, an AAO wafer, without any preprocessing, is first used as a template to introduce Au seedings on the STO substrate. In Step 2, the AAO wafer is removed, and the BTO-Au VAN film is deposited on the Au-seeded substrate. Scanning transmission electron microscopy (STEM) analysis was conducted on the BTO-Au samples with or without the Au seedings to examine the effectiveness of the AAO-templated Au seedings. Optical properties were also compared. This simple Au seeding method may open up new avenues for enhancing the pillar morphology and distribution control of other metal-oxide VAN films in general.

2. EXPERIMENTAL SECTION

2.1. Au Seedings and Composite Film Growth. The Au seedings were initially deposited via an AAO template (20 μm thick) with a pore size of 250 nm acquired from InRedox, Co., covering the STO substrate during the deposition process. The chamber was evacuated to a base pressure of 3×10^{-8} Torr. The Au seedings were generated by firing the laser (a KrF excimer laser, Lambda-Physik COMPex Pro 205, $\lambda = 248$ nm) at a Au foil and deposited at 700 °C in a vacuum ambience. The laser fluence was 3.6 J/cm^2, and the repetition rate was 5 Hz. The number of laser pulses shot on the Au foil was set to 500, 1000, and 1500, respectively.

The BTO-Au target was fabricated by blending barium titanate and Au powders in a 3:1 atomic ratio, followed by conventional sintering in a furnace at 950 °C for 6 h in air. BTO-Au nanocomposite films, both with and without Au seedings, were grown on STO (001) substrates using PLD. The deposition conditions for all BTO-Au films were optimized as detailed below. The substrate temperature was maintained at a constant 750 °C with an oxygen background pressure of 200 mTorr, using a laser fluence of 3.2 J/cm^2, and a laser frequency of 5 Hz. After deposition, the films were cooled to room temperature at a rate of 10 °C/min. The PLD setup is illustrated in Figure S1.

2.2. Microstructure Characterization. The Au seedings were characterized using scanning electron microscopy (SEM, Thermo Fisher Scientific Teneo). The microstructure and crystallinity of the samples were examined using X-ray diffraction (XRD, PANalytical Empyrean), transmission electron microscopy (TEM), and high-resolution scanning transmission electron microscopy (STEM, Thermo Fisher Scientific TALOS 200X operated at 200 kV). TEM samples were prepared through manual grinding and thinning processes, followed by dimpling and ion milling using a precision ion polishing tool (PIPS II Model 695 by Gatan). Chemical composition analysis was conducted using energy-dispersive X-ray spectroscopy (EDS) in STEM mode.

2.3. Optical Property Measurements. Transmittance measurements were performed using a UV−vis−NIR absorption spectrophotometer (PerkinElmer Lambda 1050). The dielectric permittivity was investigated through spectroscopic ellipsometry (JA Woollam RC2). The ellipsometer parameters Ψ and Δ, related by the equation $r_p/r_s = \tan(\Psi)e^{i\Delta}$ (where r_p and r_s are the reflection coefficients for the p-polarized and s-polarized light, respectively), were fitted using CompleteEASE software. The incident angle was set to 35, 45, and 55° to enhance the accuracy of the model. The dielectric permittivity was assumed to be anisotropic owing to the matrix-pillar structure. Permittivity along the in-plane (IP) and out-of-plane (OOP) directions was modeled by employing Drude and Lorentz oscillators. The fitted results exhibited a mean squared error of approximately 5. The raw data (Ψ and Δ) used to fit the permittivity is plotted in Figure S7.

3. RESULTS AND DISCUSSION

The sequential deposition process of the Au seedings and the BTO-Au films is illustrated in Figure 1. First, the 20 μm thick AAO wafer covers the surface of the STO substrate and acts as a template to assist the formation of the Au seedings. The Au adatoms contained in the plume pass through the AAO template and land on the STO substrate forming the Au seedings as observed in SEM (see Figure 2). To grow the Au seedings, the number of laser pulses was set to 500, 1000, and 1500, respectively. Figure 2 shows the SEM images of Au
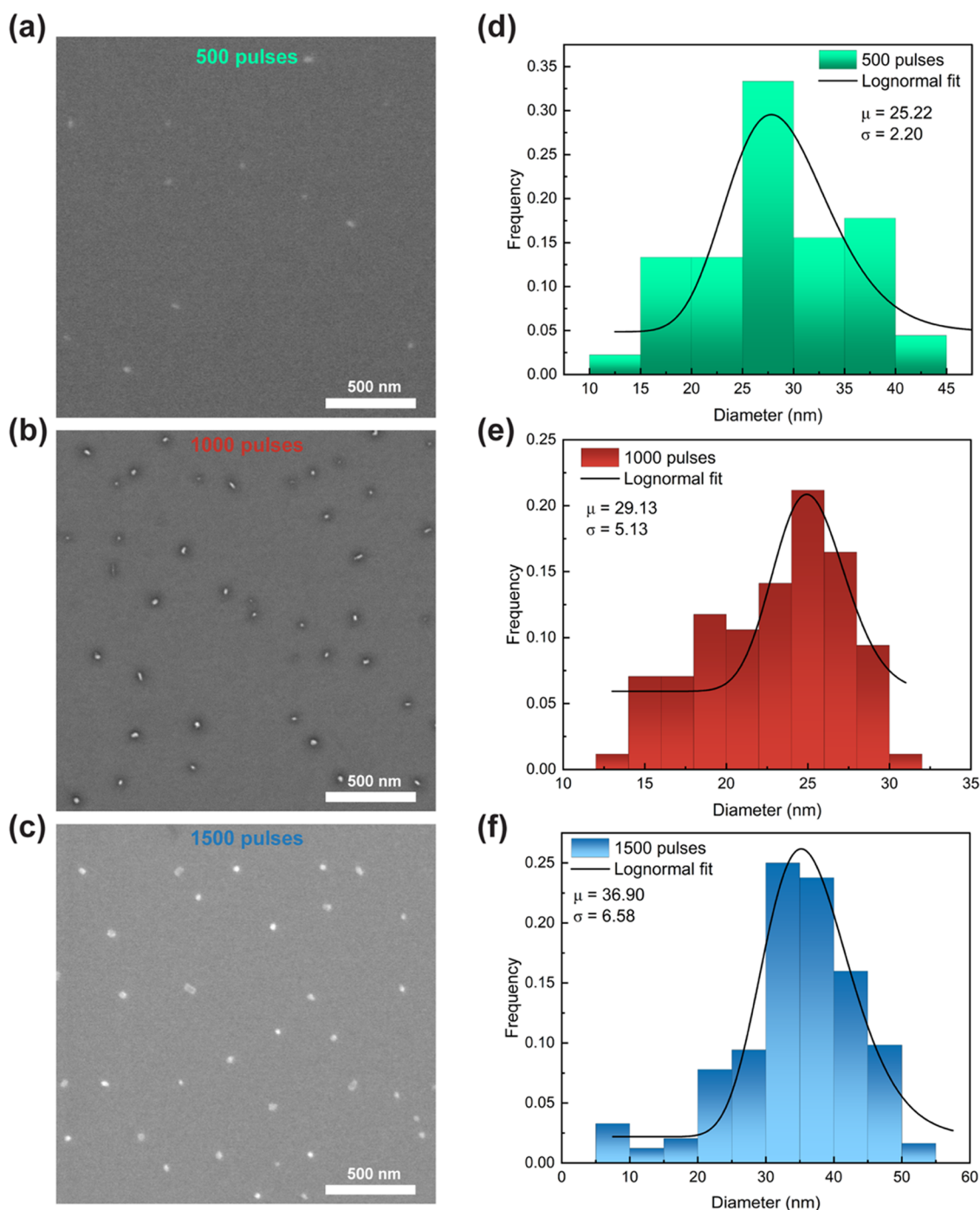
Figure 2. (a−c) SEM images of the Au seedings of 500, 1000, and 1500 laser pulses, respectively. (d−f) Diameter histogram plots of the three samples showing the diameter distributions.

seedings for the three conditions, wherein the Au seedings appear as nanoparticle-like structures of various sizes. Owing to the atomic number contrast mechanism in back-scattering electron mode, the Au seedings appear to be brighter than the substrate. The corresponding histograms for the diameters of the Au seedings are plotted in Figure 2 as well, with the diameter distributions fitted using a lognormal function. From the statistical results, a notable trend emerges, i.e., the diameter of the Au seedings increases monotonically with the number of laser pulses. The mean diameter of the Au seedings increases from 25.22 nm to 36.90 nm as the laser shots increase from 500 pulses to 1500 pulses (see Figure S6), which happens

because more Au adatoms will merge into larger Au clusters forming larger Au seedings. However, it is likely that some Au seedings that are not large enough to be resolved by SEM exist on the substrate as well and may play a role in assisting the subsequent Au pillars growth.

The mechanism of the seeding formation can be explained by the classical Volmer−Weber epitaxial film growth theory, wherein the Au adatoms follow the "island growth" mode due to their comparatively high surface energy ($\gamma = 0.71$ J/m^2 for (111) orientation).[20,21] Generally, the Au adatoms initially form numerous islands, and as they grow larger, they begin to merge with each other and form a Au layer. However, due to
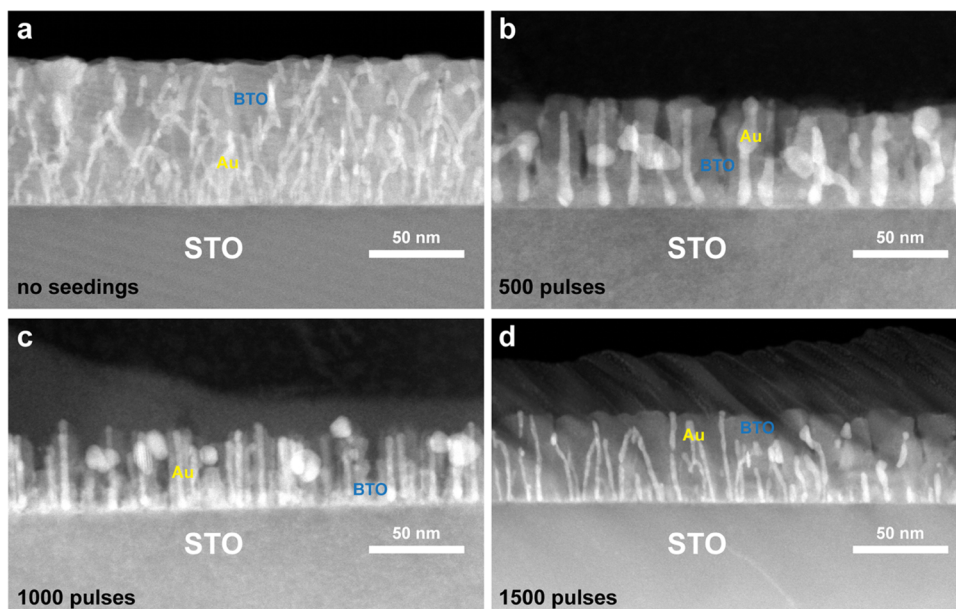
Figure 3. Cross-sectional STEM images of (a) the control sample (without Au seedings), (b) the 500-pulse Au seedings sample, (c) the 1000-pulse Au seedings sample, and (d) the 1500-pulse Au seedings sample.

the presence of the AAO template in this work, the motion of the Au adatoms is confined in space by the AAO pores. Consequently, the likelihood of the islands coalescing decreases, so the Au seedings form on the substrate rather than a Au layer. After the deposition of the Au seedings, the BTO-Au nanocomposite film was deposited on the Au seedings-covered STO substrate. Owing to the lower interfacial energy between the same atom species, the Au adatoms preferentially land on the existing Au seedings, leading to an ordered VAN structure compared to the BTO-Au films without Au seedings.

Figure 3 compares the nanostructure of the BTO-Au films grown under four different conditions: without Au seedings (a control sample), with 500, 1000, and 1500 pulses of Au seedings. Although all four STEM images show a pillar-in-matrix structure wherein the Au nanopillars with bright contrast are embedded in the BTO matrix, the BTO-Au films with Au seedings display distinct features compared to that without Au seedings. Figure 3a presents an image of the sample without the Au seedings. It is clear that the Au pillars are entangled and randomly distributed in the BTO matrix. In contrast, with the Au seedings, the Au pillars grow straighter and are more evenly distributed in the matrix, as displayed in Figure 3b–d. Interestingly, the latter films all exhibit columnar growth to some extent in terms of the BTO matrix. Specifically, the BTO tends to grow around the Au pillars, forming a core–shell-like structure, i.e., a Au core and a BTO shell, which is particularly evident in the case of 500- and 1000-pulse Au seedings samples. Such core–shell structure could be related to the accelerated Au pillar growth due to the initial Au seeds and the BTO shell nucleated around the Au pillars. In the seeding-containing films, the BTO growth tends to be guided by the well-separated Au pillars and grow around them, resulting in a less continuous growth (Figure 3b,c). On the other hand, the BTO matrix becomes more continuous when there are no well-separated Au pillars present (Figure 3a). Figure S2 presents a comprehensive comparison of the three BTO-Au films with the HRSTEM images, clearly revealing distinct structural differ-

ences among them. In Figure S3, the chemical composition of the 1500-pulse sample is shown, where the Au pillars are clearly embedded in the BTO matrix. The preferred growth orientation is determined to be BTO (001) and Au (111) as proven by the XRD result in Figure S4, which is consistent with the previous result.[22] The results clearly reveal the enhanced ordering and morphology of the Au pillars embedded in the matrix owing to the assistance of the Au seedings.

The optical properties of plasmonic metal-oxide nanocomposites have garnered significant interest due to their considerable potential as metamaterial candidates. Often, the optical properties of these VAN systems exhibit anisotropy, which results from their anisotropic structures. In this study, the IP and OOP permittivity of four samples within the near-infrared, visible, and ultraviolet regions (250−1800 nm) was investigated using spectroscopic ellipsometry, as illustrated in Figure 4. Notably, all samples display a very different permittivity dispersion along the IP and OOP directions within the measured wavelength range, which aligns with previous reports of BTO-Au.[22,23] Intriguingly, the BTO-Au film with 1000-pulse Au seedings exhibits type I ($\varepsilon_\perp < 0$, $\varepsilon_{a\parallel} > 0$) hyperbolic behavior between 290 nm and 460 nm. Such fact could be caused by the unique structure of the 1000-pulse sample, which possesses the most anisotropic matrix structure in terms of the BTO matrix discontinuity and the vertically aligned Au pillars. Consequently, the permittivity displays a negative sign along the OOP direction due to the contribution of the Au nanopillars yet remains positive along the IP direction. Furthermore, the transmittance measurement results shown in Figure S5 reveal the presence of plasmonic absorption in all samples. The improved nanostructure of the BTO-Au film makes it a promising candidate for the application of plasmonic hyperbolic metamaterial.

In this study, the use of Au seedings in BTO-Au remarkably enhances the ordering and morphology of the embedded Au pillars, compared to the samples without seedings. This technique offers a simple and clean alternative to complex or
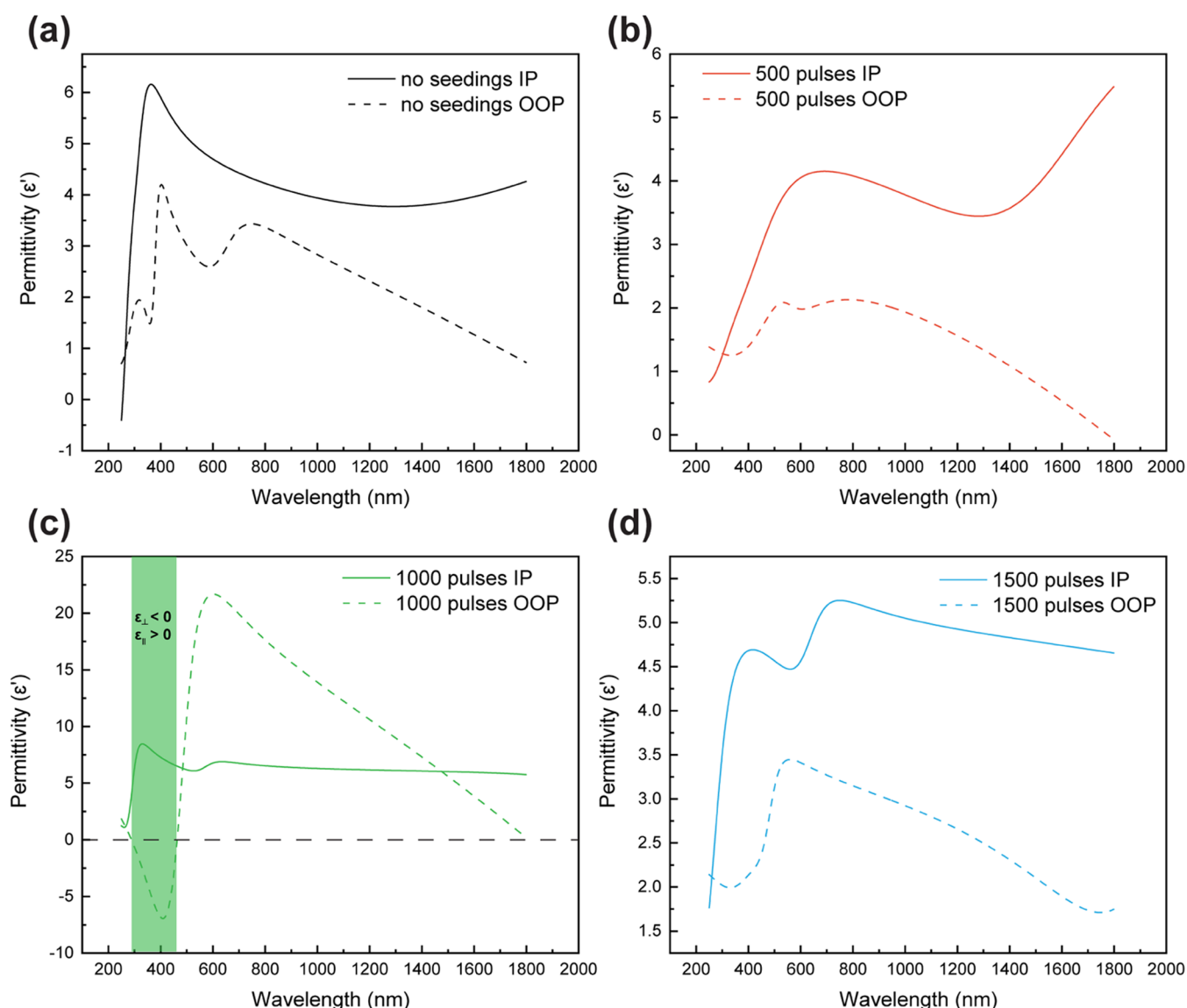
Figure 4. Permittivity dispersion of (a) the control sample and the samples with (b) 500, (c) 1000, and (d) 1500 laser pulses along the in-plane and out-of-plane directions.

chemical-intensive methods such as EBL, RIE, or chemical etching. The Au seedings, introduced through an AAO template via pulsed laser deposition, allow for a better control over the nanopillar growth, which has been a persistent challenge in the VANs growth. This innovative approach could be extended to other metal-oxide systems, encouraging the design of advanced two-phase nanocomposite materials with controlled structures. The enhanced structural control promises impactful future developments, such as directed nucleation and growth for specific on-chip integration of VAN systems for future devices.

4. CONCLUSIONS

In conclusion, utilizing a porous AAO template to introduce Au seedings on the STO substrate can enhance the ordering and morphology of the Au nanopillars embedded in the BTO matrix, with the diameter of Au seedings increasing as the number of laser pulses increases. In contrast to the entangled and randomly distributed Au nanopillars found in BTO-Au films without the Au seedings, the Au nanopillars can grow

much straighter and more orderly with the assistance of Au seedings owing to the low interfacial energy between the same atom species. The BTO-Au films with Au seedings exhibit a core—shell-like structure, with the BTO matrix showing a columnar growth guided by the Au nanopillars. Furthermore, the 1000-pulse sample displays hyperbolic dispersion within the range of 290−460 nm, making it a promising metamaterial candidate for future optical applications. This demonstration presents the feasibility of Au seeding for well-controlled oxide-metal VAN growth and potential for directed growth of VANs for on-chip integration. The findings lay a solid foundation for exploring the untapped potential of VANs in advanced technological applications.

■ ASSOCIATED CONTENT

Data Availability Statement

The data sets produced and/or examined in the course of this research can be obtained from the corresponding author upon a reasonable request.

Supporting Information

The Supporting Information is available free of charge at https://pubs.acs.org/doi/10.1021/acsomega.3c04701.

Conceptual drawing of the deposition setup; high-angle annular dark-field scanning transmission electron microscopy (HAADF-STEM) images; HAADF energy-dispersive X-ray spectroscopy (EDS) mapping images; raw data for ellipsometry measurements; and transmittance measurements (PDF)

(PDF)

AUTHOR INFORMATION

Corresponding Author

Haiyan Wang − *School of Materials Engineering, Purdue University, West Lafayette, Indiana 47907, United States; Elmore Family School of Electrical and Computer Engineering, Purdue University, West Lafayette, Indiana 47907, United States;* orcid.org/0000-0002-7397-1209; Email: hwang00@purdue.edu

Authors

Jianan Shen − *School of Materials Engineering, Purdue University, West Lafayette, Indiana 47907, United States*

Zedong Hu − *Elmore Family School of Electrical and Computer Engineering, Purdue University, West Lafayette, Indiana 47907, United States*

Lizabeth Quigley − *School of Materials Engineering, Purdue University, West Lafayette, Indiana 47907, United States*

Complete contact information is available at:
https://pubs.acs.org/10.1021/acsomega.3c04701

Author Contributions

J.S. and H.W. conceived the idea, designed all of the experiments, and formulated the mechanistic understanding. J.S. implemented the depositions and the S/TEM characterization work, conducted the optical property measurements, and completed all of the conceptual drawings. Z.H. and L.Q. contributed to the TEM sample preparation work. H.W. provided the experimental funding for the project. J.S. drafted the manuscript and all authors have given comments and suggestions on the manuscript. All authors have given approval to the final version of the manuscript.

Notes

The authors declare no competing financial interest.

REFERENCES

(1) Au, K.; Gao, X. S.; Wang, J.; Bao, Z. Y.; Liu, J. M.; Dai, J. Y. Enhanced Resistive Switching Effect in Ag Nanoparticle Embedded BaTiO3 Thin Films. *J. Appl. Phys.* **2013**, *114*, No. 027019.

(2) Schuler, V.; Milano, J.; Coati, A.; Vlad, A.; Sauvage-Simkin, M.; Garreau, Y.; Demaille, D.; Hidki, S.; Novikova, A.; Fonda, E.; Zheng, Y.; Vidal, F. Growth and Magnetic Properties of Vertically Aligned Epitaxial CoNi Nanowires in (Sr, Ba)TiO3 with Diameters in the 1.8−6 Nm Range. *Nanotechnology* **2016**, *27*, No. 495601.

(3) Schuler, V.; Bonilla, F. J.; Demaille, D.; Coati, A.; Vlad, A.; Garreau, Y.; Sauvage-Simkin, M.; Novikova, A.; Fonda, E.; Hidki, S.; Etgens, V.; Vidal, F.; Zheng, Y. Huge Metastable Axial Strain in Ultrathin Heteroepitaxial Vertically Aligned Nanowires. *Nano Res.* **2015**, *8*, 1964−1974.

(4) Zhang, D.; Gao, X.; Lu, J.; Lu, P.; Deitz, J.; Shen, J.; Dou, H.; He, Z.; Shang, Z.; Wade, C. A.; Zhang, X.; Chen, A.; Wang, H. Novel Self-Assembled Two-Dimensional Layered Oxide Structure Incorporated with Au Nanoinclusions towards Multifunctionalities. *Nano Res.* **2022**, 1465−1472.

(5) Kawasaki, S.; Takahashi, R.; Yamamoto, T.; Kobayashi, M.; Kumigashira, H.; Yoshinobu, J.; Komori, F.; Kudo, A.; Lippmaa, M. Photoelectrochemical Water Splitting Enhanced by Self-Assembled Metal Nanopillars Embedded in an Oxide Semiconductor Photoelectrode. *Nat. Commun.* **2016**, *7*, No. 11818.

(6) Shen, J.; He, Z.; Zhang, D.; Lu, P.; Deitz, J.; Shang, Z.; Kalaswad, M.; Wang, H.; Xu, X.; Wang, H. Tunable Physical Properties in Bi-Based Layered Supercell Multiferroics Embedded with Au Nanoparticles. *Nanoscale Adv.* **2022**, *4*, 3054−3064.

(7) He, Z.; Qi, Z.; Yang, B.; Lu, P.; Shen, J.; Dilley, N.; Zhang, X.; Wang, H. Controllable Phase Transition Properties in VO2 Films via Metal-Ion Intercalation. *Nano Lett.* **2023**, *23*, 1119−1127.

(8) Zhang, Y.; Song, J.; Lu, P.; Deitz, J.; Zhang, D.; Dou, H.; Shen, J.; Hu, Z.; Zhang, X.; Wang, H. Tunable Magnetic and Optical Anisotropy in ZrO2-Co Vertically Aligned Nanocomposites. *Adv. Mater. Interfaces* **2023**, *10*, No. 2300150.

(9) MacManus-Driscoll, J. L.; Wu, R.; Li, W. Interface-Related Phenomena in Epitaxial Complex Oxide Ferroics across Different Thin Film Platforms: Opportunities and Challenges. *Mater. Horiz.* **2023**, *10*, 1060−1086.

(10) Misra, S.; Wang, H. Review on the Growth, Properties and Applications of Self-Assembled Oxide-Metal Vertically Aligned Nanocomposite Thin Films-Current and Future Perspectives. *Mater. Horiz.* **2021**, *8*, 869−884.

(11) Lu, J.; Paldi, R. L.; Pachaury, Y.; Zhang, D.; Wang, H.; Kalaswad, M.; Sun, X.; Liu, J.; Phuah, X. L.; Zhang, X.; El-Azab, A. A.; Wang, H. Ordered Hybrid Metamaterial of La0.7Sr0.3MnO3−Au Vertically Aligned Nanocomposites Achieved on Templated SrTiO3 Substrate. *Mater. Today Nano* **2021**, *15*, No. 100121.

(12) Aimon, N. M.; Choi, H. K.; Sun, X. Y.; Kim, D. H.; Ross, C. A. Templated Self-Assembly of Functional Oxide Nanocomposites. *Adv. Mater.* **2014**, *26*, 3063−3067.

(13) Dong, G.; Wang, T.; Liu, H.; Zhang, Y.; Zhao, Y.; Hu, Z.; Ren, W.; Ye, Z. G.; Shi, K.; Zhou, Z.; Liu, M.; Pan, J. Strain-Induced Magnetoelectric Coupling in Fe3O4/BaTiO3 Nanopillar Composites. *ACS Appl. Mater. Interfaces* **2022**, *14*, 13925−13931.

(14) Stratulat, S. M.; Lu, X.; Morelli, A.; Hesse, D.; Erfurth, W.; Alexe, M. Nucleation-Induced Self-Assembly of Multiferroic BiFeO3−CoFe2O4 Nanocomposites. *Nano Lett.* **2013**, *13*, 3884−3889.

(15) Comes, R.; Liu, H.; Khokhlov, M.; Kasica, R.; Lu, J.; Wolf, S. A. Directed Self-Assembly of Epitaxial CoFe2O4−BiFeO3 Multiferroic Nanocomposites. *Nano Lett.* **2012**, *12*, 2367−2373.

(16) Dong, G.; Zhou, Z.; Guan, M.; Xue, X.; Chen, M.; Ma, J.; Hu, Z.; Ren, W.; Ye, Z.-G.; Nan, C.-W.; Liu, M. Thermal Driven Giant Spin Dynamics at Three-Dimensional Heteroepitaxial Interface in Ni0.5Zn0.5Fe2O4/BaTiO3-Pillar Nanocomposites. *ACS Nano* **2018**, *12*, 3751−3758.

(17) Hao, Q.; Huang, H.; Fan, X.; Hou, X.; Yin, Y.; Li, W.; Si, L.; Nan, H.; Wang, H.; Mei, Y.; Qiu, T.; Chu, P. K. Facile Design of

Ultra-Thin Anodic Aluminum Oxide Membranes for the Fabrication of Plasmonic Nanoarrays. *Nanotechnology* **2017**, *28*, No. 105301.

(18) Zhang, Y.; Zhang, D.; Liu, J.; Lu, P.; Deitz, J.; Shen, J.; He, Z.; Zhang, X.; Wang, H. Self-Assembled HfO2 -Au Nanocomposites with Ultra-Fine Vertically Aligned Au Nanopillars. *Nanoscale* **2022**, *14*, 11979−11987.

(19) Misra, S.; Li, L.; Zhang, D.; Jian, J.; Qi, Z.; Fan, M.; Chen, H.; Zhang, X.; Wang, H. Self-Assembled Ordered Three-Phase Au−BaTiO3−ZnO Vertically Aligned Nanocomposites Achieved by a Templating Method. *Adv. Mater.* **2019**, *31*, No. 1806529.

(20) Jain, A.; Ong, S. P.; Hautier, G.; Chen, W.; Richards, W. D.; Dacek, S.; Cholia, S.; Gunter, D.; Skinner, D.; Ceder, G.; Persson, K. A. Commentary: The Materials Project: A Materials Genome Approach to Accelerating Materials Innovation. *APL Mater.* **2013**, *1*, No. 011002.

(21) Tran, R.; Xu, Z.; Radhakrishnan, B.; Winston, D.; Sun, W.; Persson, K. A.; Ong, S. P. Surface Energies of Elemental Crystals. *Sci. Data* **2016**, *3*, No. 160080.

(22) Zhang, D.; Misra, S.; Li, L.; Wang, X.; Jian, J.; Lu, P.; Gao, X.; Sun, X.; Qi, Z.; Kalaswad, M.; Zhang, X.; Wang, H. Tunable Optical Properties in Self-Assembled Oxide-Metal Hybrid Thin Films via Au-Phase Geometry Control: From Nanopillars to Nanodisks. *Adv. Opt. Mater.* **2020**, *8*, No. 1901359.

(23) Liu, J.; Wang, X.; Gao, X.; Wang, H.; Jian, J.; Huang, J.; Sun, X.; Qi, Z.; Misra, S.; He, Z.; Wang, H. Multifunctional Self-Assembled BaTiO3-Au Nanocomposite Thin Films on Flexible Mica Substrates with Tunable Optical Properties. *Appl. Mater. Today* **2020**, *21*, No. 100856.